SEVEN publicações acadêmicas
EM PARCERIA COM: IEMS UNIASSELVI

Comparison between the characteristics wing and empennage aerodynamics horizontal in competition aircraft aerodesign SAE - Brasil

Kelmy Ângelo de Figueiredo Alves[1], Luis Morão Cabral Ferro[2].

ABSTRACT

This article presents the comparative analysis of the aerodynamic behavior of the wing and empennage or horizontal stabilizer for small aircraft characteristic of the SAE Aerodesign competition. The software used to calculate the aerodynamic characteristics of the sustaining elements was XFLR5. The objective of the research was the selection of the most suitable aerodynamic profiles of the horizontal stabilizer, aiming to improve the performance and efficiency of aircraft designed for low speeds. Using the XFLR5, with the vortex mesh method, several aerodynamic aspects were analyzed, such as the curves of the lift coefficient, the lift coefficient as a function of the drag coefficient, the moment coefficient and the aerodynamic efficiency as a function of the angle of attack. The profile selected for the wing was the Selig 1223 RTL and for the horizontal empennage the NACA0012H, NACA0012 and NACA2412 profiles. Calculations were made for the flow around the wing, around the three horizontal empennages and around the three wing combinations with the different empennage geometries. Results are presented regarding the evolution of aerodynamic coefficients and aerodynamic efficiency with the angle of attack for the geometries already mentioned.

Keywords: Aerodynamics, Wing profile, Horizontal empennage, XFLR5, Comparative analysis, Aerodynamic performance.

INTRODUCTION

Since 2013, UFERSA has had an Aerodesign team that participates annually in the SAE Aerodesign competition in Brazil. The design of an aircraft for participation in the competition involves different subsystems, such as Aerodynamics, Loads and Aeroelasticity, Structures, Stability and Control, Performance and Electrical.

The success of the participation depends on a good design of the aircraft. A good aerodynamic design is essential for the aircraft to have good behavior in flight. The computational analysis of the flow around the supporting elements allows a determination of the aerodynamic characteristics of the aerodynamic components, in particular the wing and the horizontal stabilizer. The joint calculation of the flow around the wing and the horizontal stabilizer makes it possible to analyze the aerodynamic stability of the aircraft.

The flow around the elements can be calculated using different methodologies. Among the

[1] Undergraduate student of the Bachelor's Degree in Mechanical Engineering, UFERSA, Mossoró – RN
[2] Associate Professor – UFERSA, Mossoró – RN

most used are the Lifting Line method (Anderson, 2010), the panel method (HESS, 1976) and the Vortex Lattice Method (VLM) (THOMAS, 1976). These methods are integral methods and therefore do not require domain discretization. On the contrary, other methods, such as the Finite Volume Method (HIRSH, 2007), require the definition of a domain and its discretization with the generation of a mesh. In addition, it is still necessary to use a turbulence model. These methods are more complex to use and consume much more CPU time than the full methods, making their use in design, where it is necessary to perform many simulations impractical unless computers with high computational capacity are available.

The use of computer codes to calculate the three-dimensional flow of the supporting elements, wing and stabilizers allows a better knowledge of the flow around these elements and the determination of the forces and moments and also the surface pressure distributions that play a fundamental role with regard to flight performance and efficiency.

In the present article, the software used was XFRL5 (Drela, 1989; XFLR5), which its authors describe as "XFLR5 is an analysis tool for airfoils, wings, and airplanes operating with low Reynolds numbers. Includes: XFOIL forward and inverse analysis capabilities (Drela et al 2001) and wing design and analysis capabilities based on Lift Line Theory, the Vortex Mesh Method, and the Three-Dimensional Panel Method"

Using the VLM method, the three-dimensional invised flow around the supporting elements, wing and horizontal empennage, of an aircraft of the PegAzuls Aerodesign team was calculated. The wing is rectangular with a Selig 1223 RTL profile, using the VLM method of the XFLR5 code. The same code was also used to calculate the flow around the horizontal empennages with three different geometries using the NACA0012, NACA0012H and NACA2412 profiles. In the final part of the article, comparative results for the flow around the wing and horizontal empennage combinations are presented: S1223 RTL × NACA0012H, S1223 RTL × NACA0012 and S1223 RTL × NACA2412.

THEORETICAL BACKGROUND

In cruising flight conditions, the lift force is in equilibrium with the weight of the aircraft and the pulling force (forward) produced by the engine with the drag force, as shown in Figure 1.

Figure 1 – Forces acting on an aircraft in cruise flight.

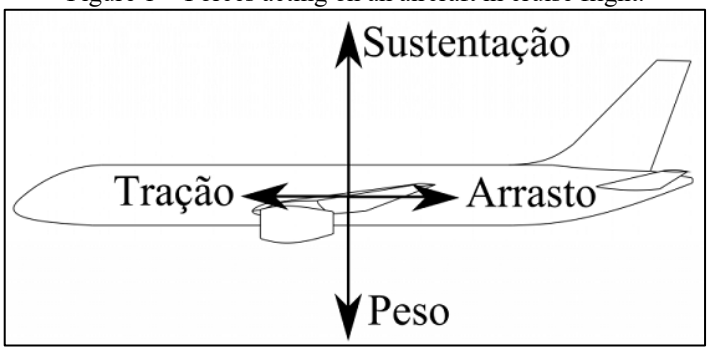

Source: Sorbilli, 2018

The elements that generate lift forces are the wings and the horizontal stabilizer (empennage) (Sorbilli, 2018). The tractive force is generated by the propellant. Drag is the force of resistance generated by the aircraft to movement. In three-dimensional flow around the supporting element, there is drag induced by the flow originating at the end of the wing due to the pressure difference between the soffit and the extradosis (Brederode, 2018).

SUSTAINING FORCES

Lift force represents the highest quality an aircraft possesses compared to other types of vehicles and defines an airplane's ability to stay in flight. The lift force is used as a way to overcome the weight of the aircraft and thus ensure flight (Miranda, 2011). To represent the lifting force, the symbol L will be used. The lifting force originates from the non-symmetrical distribution of pressure with pressures in the extradossum lower than the pressure of the approach flow, $p\square$, and in the soffit greater than $p\square$. The reduction of pressure in the soffit increases with the angle of attack α and with the increase of the curvature of the profile (Miranda, 2011).

The lift force increases with the angle of attack □, varying linearly with □, for small angles, reaching its maximum value for the stall angle. From the stall angle, the lift coefficient begins to decrease. The intensity of the lift force, in non-viscous flow, is proportional to the angle of attack □. For the same angle of attack, profiles with greater curvature have higher lift coefficients.

DRAG FORCE

In the drag force *D* on an aircraft, two types can be considered, parasitic drag and induced drag. Parasitic drag is the result of pressure and viscous forces exerted by aircraft components, such as wing, horizontal and vertical stabilizers, fuselage, landing gear, etc., in the opposite direction to its displacement.

The induced drag is characterized as a pressure drag and is generated by the wingtip vortices that produce a disturbed flow field over the wing and interfere with the pressure distribution over the wing surface, causing an extra drag component in relation to the aerodynamic profile (Miranda, 2011). The induced drag causes a downward velocity, decreasing the angle of attack of the approach flow (Anderson, 2010).

ANGLE OF ATTACK

The angle of attack □ is the angle formed between the line of the profile chord and the direction of the approach flow, upstream velocity of the aircraft. The increase in the angle of attack provides an increase in lift force until the angle corresponding to the maximum lift is reached, stall angle, from which the lift decreases sharply.

The increase in the angle of attack also provides a variation in the drag force generated by the profile. This dependence between lift and drag can be measured through the aerodynamic efficiency of the profile given by the ratio between the lift coefficients *cl* and drag *coefficients cd*.

SIZING AND SIMULATION

The XFLR5 code is a tool for the analysis of profiles, wings and aircraft in low Reynolds number runs. The XFLR5 includes the two-dimensional XFOIL code that performs direct and inverse aerodynamic analysis on airfoil and codes for the design and analysis of supporting elements by the methods of the sustaining line theory (Anderson, 2010), vortex mesh method or three-dimensional panel method (HESS, 1966).

In the vortex mesh (VLM) method, the curvature surface or the surface containing the chord of the profiles in trapezoidal shaped panels. In each panel there is a vortex connected in the shape of a horseshoe positioned 1/4 of the way down the panel chord, as can be seen in Figure 2. The velocities induced by the vortex filaments are calculated using the Biot-Savart law. The intensity of the horseshoe vortices is calculated from the imposition of the boundary condition specified at the control points of the various panels. The control points are placed in the central plane of the panel at a distance of 3/4 of the panel chord from the leading edge of the panel. The dragged vortices generate a wake that can be approximated by a fixed flat belt, simpler modeling, or by a curved belt aligned with the current surface that comes out of the trailing edge of the wing, a situation that gives rise to an iterative procedure (Brederode, 2018).

Figure 2 – Modeling of a wing with horseshoe vortices and location of control points.

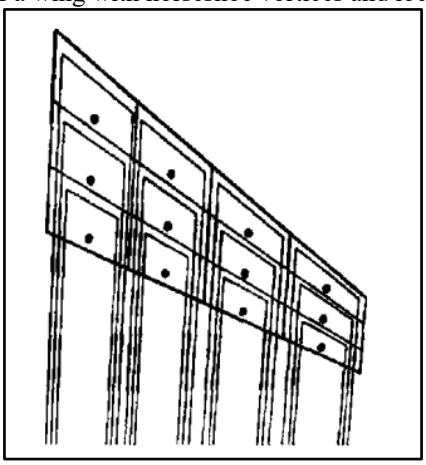

Font: Brederode, 2018

To calculate the three-dimensional flow around the supporting elements, the XFLR5 v6.59 softwares and the VLM vortex mesh method were used. The wing surface was discretized into 494 panels for the modeling of the wing only and 760 panels were used to simulate the flow in the wing configuration and horizontal empennage simultaneously.

To run the program, you must first define the geometry. It was considered that the wing was rectangular, as shown inFigure 3, whose construction is easy and its construction cost is considerably low when compared to other geometries. The wing has a wingspan of 2 m and a chord of 0.500 m. The wing has neither twist nor sweep. The horizontal empennage, which is also rectangular, has a wingspan of 0.4 m and a rope of 0.2 m. The wing and horizontal empennage have neither twist nor sweep.

Figure 3 – Model used in 3D simulation for SELIG 1223 and NACA 2412 profiles

Source: software XFLR5

As already mentioned, the profile used for the wing was SELIG 1223 (Airfoil Tools, 2014). This profile is characterized by having a high maximum lift coefficient, close to 2.0 and a *cl*/*cd* ratio with maximum values higher than 1.2. Figure 4 shows the wing with the profile used SELIG

1223.

Figure 4 - Modeling of the wing with the Selig 1223 profile showing the discretization used.

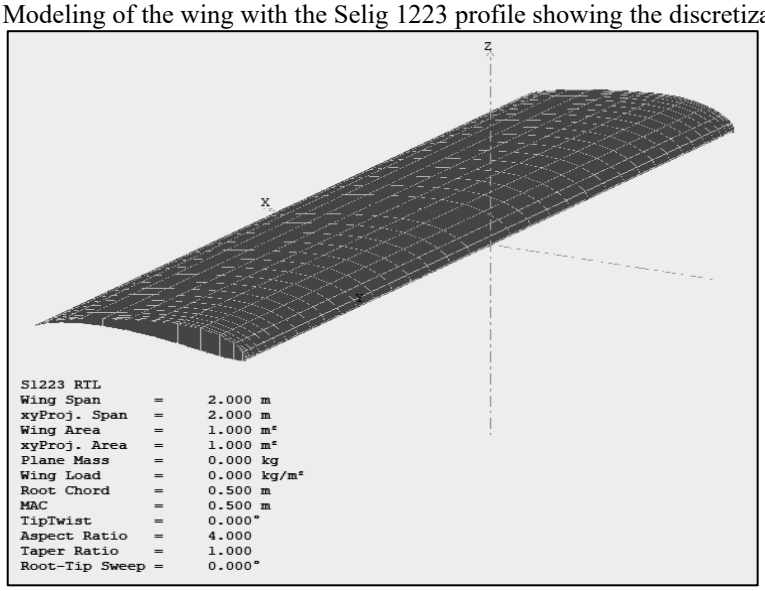

Source: Software XFLR5

The profiles chosen for the horizontal empennage were NACA0012, NACA0012H (Sheldahl, 1981) and NACA2412. All profiles have a relative thickness of 12%, with the first two being symmetrical. As can be seen in Figure 5 where an empennage with the NACA 0012H profile is represented.

Figure 5 – Modeling of the wing empennage with the NACA 0012H profile showing the discretization used.

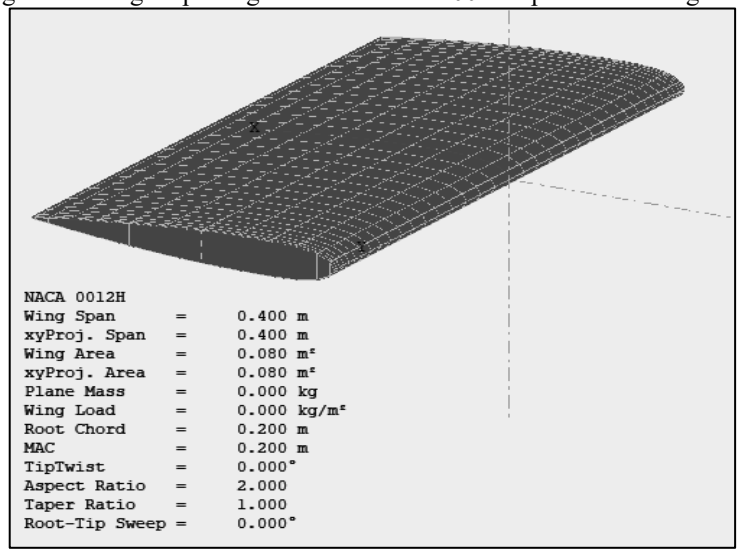

Source: software XFLR5

RESULTS

In this section, the results for the non-viscous three-dimensional flow around the wing and wingspan are presented, calculated separately and together, considering the interaction between

the wing and the horizontal empennage.

By way of reference, it is indicated that the speed of the aircraft is 16 m/s, which corresponds to a Reynolds number of the order of×5,105 and a Mach number of 0.059, which allows us to state that the flow is incompressible. In the simulations carried out, the angle of attack was between a minimum value of -10° and a maximum of 20°.

HORIZONTAL FEATHERING

The first results were obtained for the horizontal empennage, comparing the aerodynamic performance of the horizontal empennage for the three profiles already mentioned, *NACA 0012*, *NACA 0012H* and *NACA 2412*.

Lift Coefficient

Figure 6 compares the evolution of the CL lift coefficient of the horizontal empennage as a function of the angle of attack α for the three configurations.

Figure 6 – Variation of the coefficients of support of the horizontal empennage with the angle α

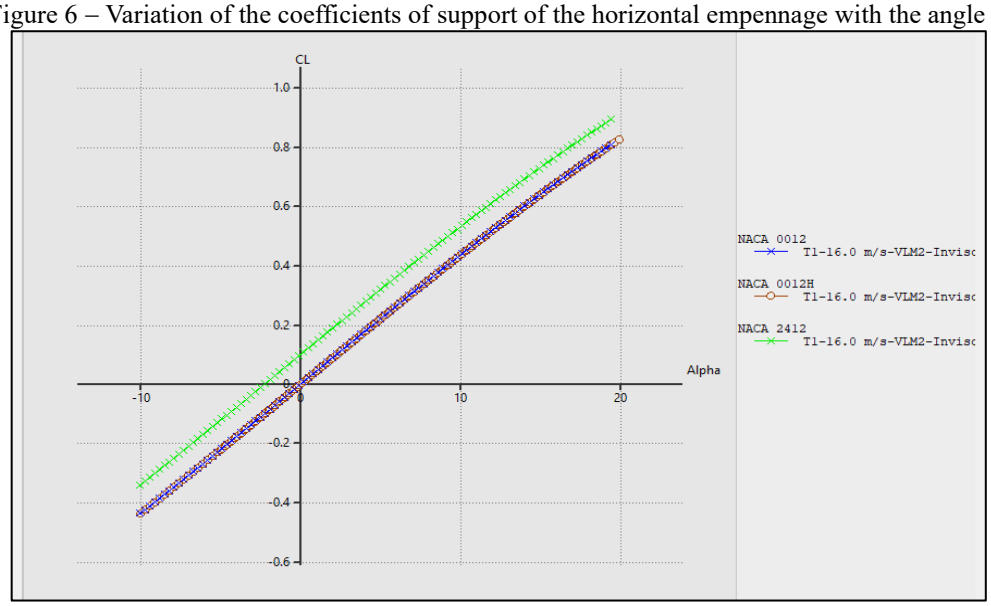

Source: Software XFLR5

The three representations have equal slopes for all three profiles. As can be seen, the empennages with the *NACA 0012* and *NACA 0012H* profiles showed graphically coincident evolutions. The NACA *2412* profile empennage has higher values for the lift coefficient due to the fact that the profile has non-zero curvature, presenting a positive lift coefficient for an angle of attack α=0°. Table 1 shows the values of the maximum lift coefficients, obtained for an angle α= 20°.

Table 1 – Maximum lift coefficient for the different empennage geometries

Aerodynamic profile	Maximum lift coefficient (*CLmax*)
NACA 0012H	0,824
NACA 0012	0,805
NACA 2412	0,891

Source: The authors

Arrasto coefficient

The comparative analysis between the drag coefficients *CD* between the horizontal empennage profiles is shown in Figure 7.

Figure 7 – Variation of horizontal empennage drag coefficients as a function of α

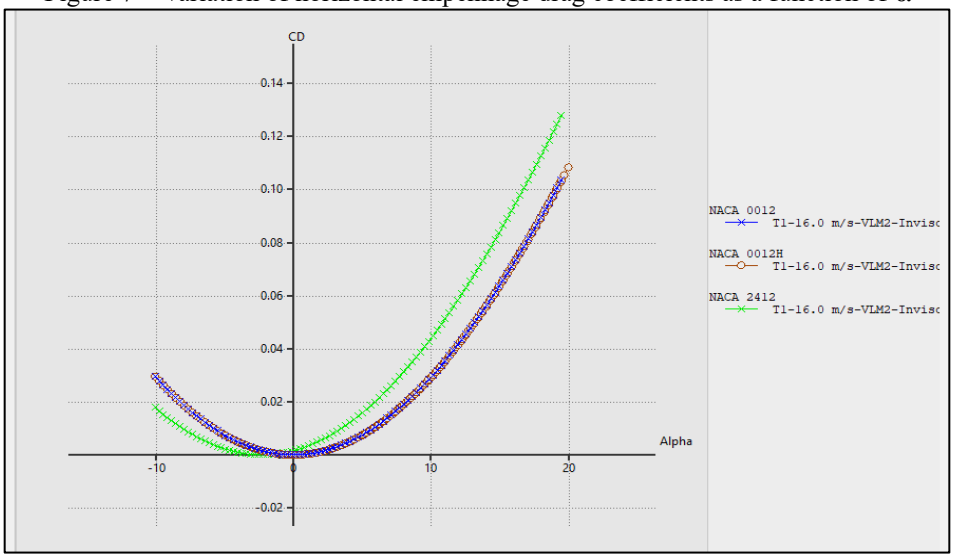

Source: Software XFLR5

When looking at the diagram, it can be seen once again that the empennages with the *NACA 0012* and *NACA 0012H* profiles have a graphic overlap. However, the *NACA 2412* profile has, for the same positive angle of attack, a higher drag coefficient than the horizontal empennages using the NACA 0012 profiles. For negative angles of attack, the opposite situation occurs. Table 2 shows the values of the maximum drag coefficients, obtained for an angle $\alpha = 20°$.

Table 2 – Maximum drag coefficient for the different empennage geometries

Aerodynamic profile	Maximum drag coefficient (*CDmax*)
NACA 0012H	0,108
NACA 0012	0,103
NACA 2412	0,128

Source: The authors

Moment Coefficient

Figure 8 shows the variation of the aerodynamic moment coefficients as a function of the

angle of attack α.

Figure 8 – Variation of horizontal empennage moment coefficients as a function of α

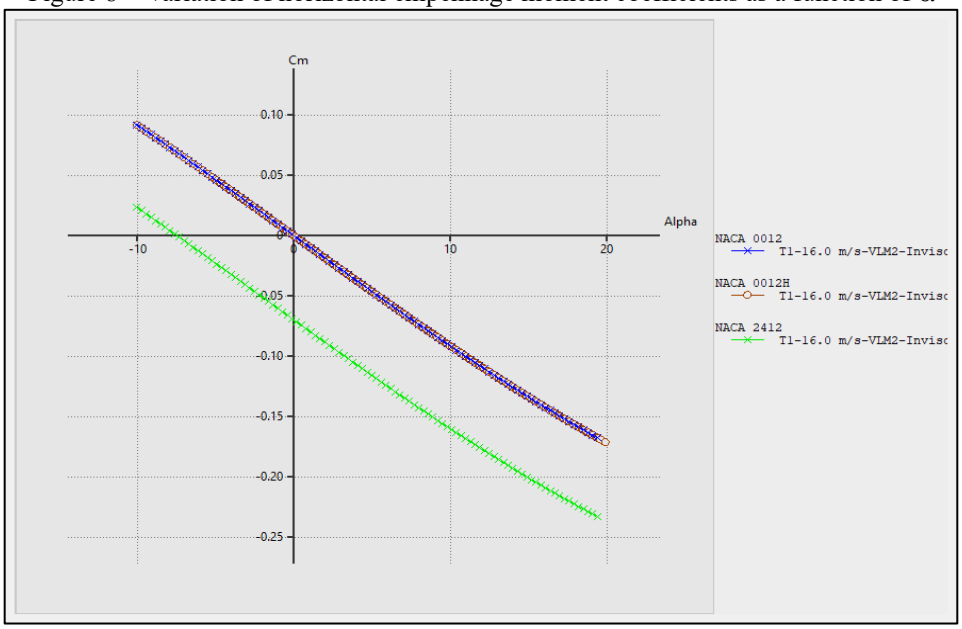

Source: Software XFLR5

A similar analysis of drag coefficients can be made in relation to moment coefficients, which are known to be related to the control and stability of the aircraft. The *NACA 0012* and *NACA0012H* profiles have overlapping evolutions of the coefficient of moment with the angle of attack. The moment coefficient when using the NACA 2412 profile has, for the same angle of attack, a moment coefficient with a higher absolute value. Table 3 shows the maximum values, in absolute value, of the moment coefficient for the three geometries of the horizontal empennage.

Table 3 – Maximum Moment Coefficient for the Different Epennage Geometries

Aerodynamic profile	**Maximum Moment Coefficient (*CMmax*)**
NACA 0012H	-0.171
NACA 0012	-0.168
NACA 2412	-0.233

Source: The authors

ASA

The aerodynamic behavior of the wing was analysed by simulation using the VLM method for the wing with the dimensions already mentioned, with the profile imposed on the wing, SELIG 1223 RTL as shown in Figure 4. As noted in Section 3, the wing has a wingspan *b* of 2 m and a *constant c* chord of 0.5 m to which corresponds an aspect ratio of 4. Figure 9 shows the evolution of the lift coefficient *CL* with the angle of attack α (9a), the drag coefficient *CD* with the angle of attack α (9b), the moment coefficient *CM* with the angle α (9c) and the aerodynamic efficiency *of*

the CL/CD wing (9d).

Figura 9 – Variação dos coeficientes aerodinâmicos da asa com o ângulo α: (a) *CL*; (b) *CD*;(c) *CM* e (d) *CL/CD*

(a) (b)

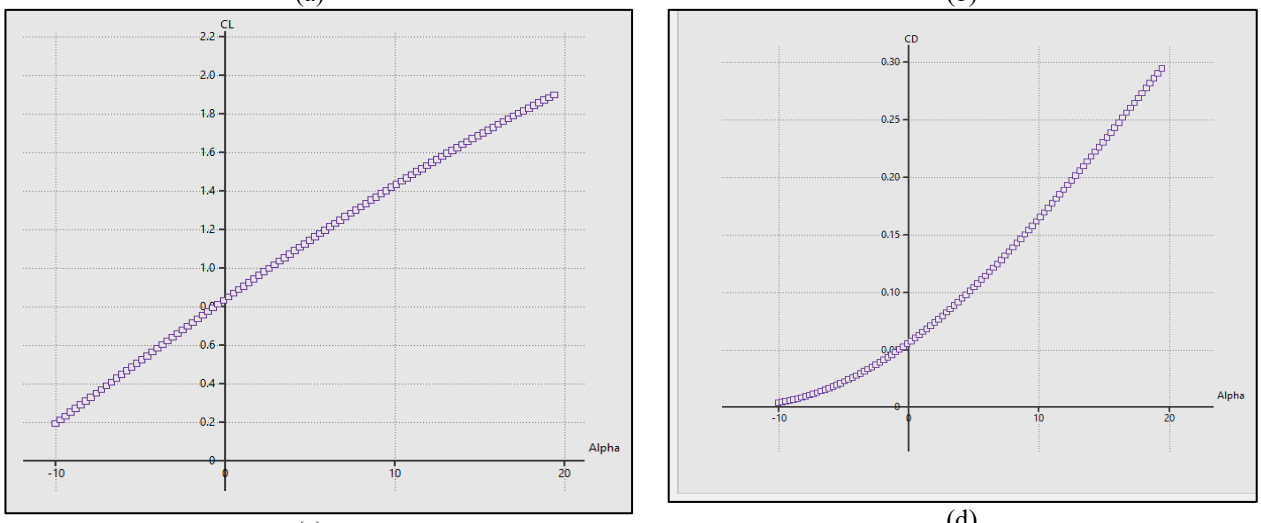

(c) (d)

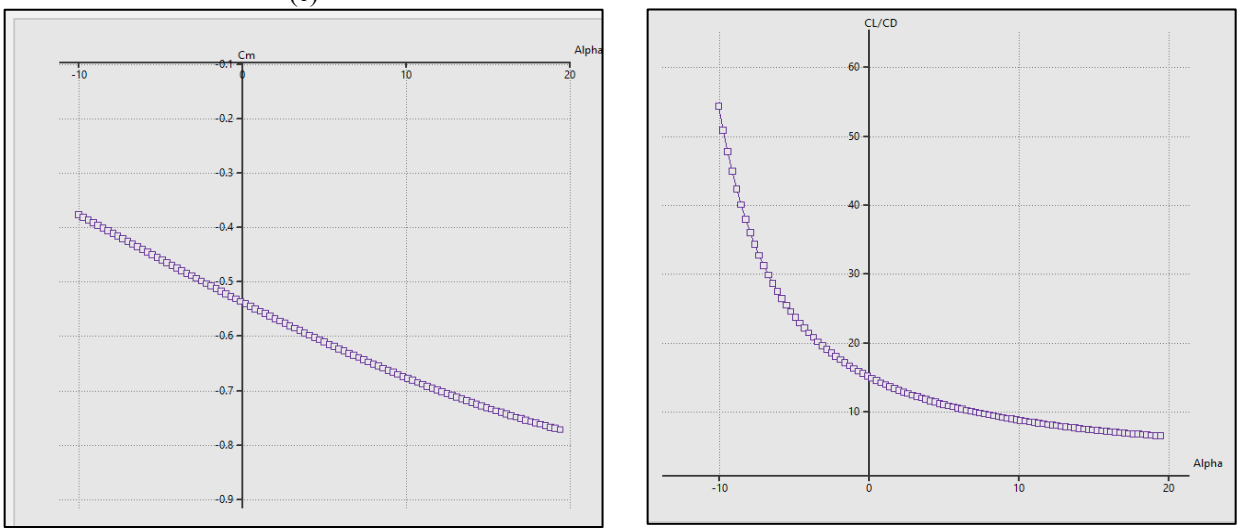

Source: Software XFLR5

By looking at Figure 9, it is possible to see that the lift coefficient has a linear evolution for angle of attack up to approximately α=12°, showing a reduction, in relation to the linear evolution, for angles α greater than 12° - Figure 9(a). The drag curve shows a slow growth for angle of attack less than 3° and linear evolution with the angle α from 3º - Figure 9(b). Figure 9(c) shows the graph of the variation of the coefficient of moment with the angle of attack. The curve shows a linear evolution for angles of attack α< 10° and a smoother evolution from α=10°. The curve presents a negative slope that means that the aircraft generates a negative moment with the increase in the angle of attack trying to reposition the aircraft in its equilibrium position (RODRIGUES, 2011). Figure 9(d) shows the evolution of the *CL/Cd ratio* as a function of the

angle of attack α= -10° and reduces rapidly. The CL/*Cd aerodynamic efficiency* is maximum for α=-10°, with an approximate value of *CL*/*Cd=54* rapidly decreasing to a *CL*/*Cd value* of 20 for an angle of attack of -4°; the minimum value occurs for the maximum angle of attack and is approximately seven.

Table 4 shows all the maximum absolute values of the aerodynamic coefficients and the efficiency for the wing with the S1223 RTL profile.

Table 4 – Maximum drag coefficient for the wing with the SELIG 1223 RTL profile

Aerodynamic coefficient	**Value**
CL	1.894
CD	0.294
CM	-0.771
CL/CD	54.25

Source: The authors

WING AND HORIZONTAL EMPENNAGE

The results of the joint modeling of the wing, with the S1223 RTL profile, and of the horizontal empennage are presented below. The three variations of profiles in the horizontal empennage already mentioned, *NACA 0012*, *NACA 0012H* and *NACA 2412*, were considered. This comparison aims to choose the best horizontal wing-empennage set according to the parameters pre-established by the project.

Lift Coefficients

Initially, the comparative lift between the three configurations of wing and empennage was analyzed. Figure 10 shows the evolution of the lift coefficient with the angle of attack α for the three configurations. As can be seen, the three combinations have very similar evolutions. By the way, it is mentioned that it is not possible to visualize the *stall* point, since in the *VLM analysis* the fluid is considered inviscid. From the graph in the figure referred to, it is possible to see that the *S1223 × NACA 0012H combination,* represented by the blue color in Figure 10, has slightly higher lift coefficients than the others, obtaining for this combination a maximum lift coefficient value higher than the others, as shown in Table 5.

Figure 10 – Comparison of the evolution of the lift coefficient as a function of the angle of attack for the three wing and horizontal empennage combinations

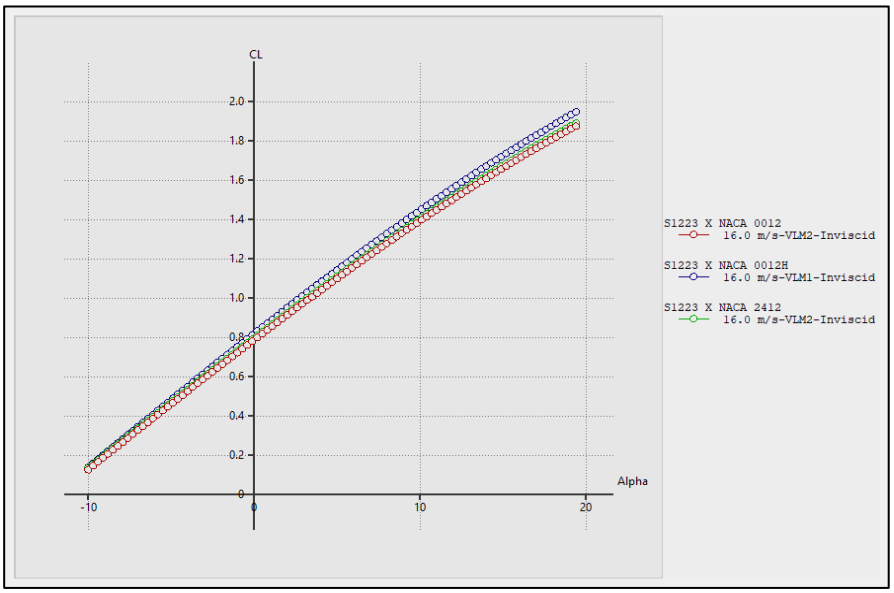

Source: Software XFLR5

Table 5 – Maximum lift coefficients for the three configurations: wing and horizontal empennage

Configuration	**Maximum lift coefficient (*CLmax*)**
S1223 RTL com NACA 0012H	1.943
S1223 RTL com NACA 0012	1.870
S1223 RTL com NACA 2412	1.886

Source: The authors

Drag Coefficients

Figure 11 shows the comparison of the evolution of the drag coefficient as a function of the angle of attack for the three geometries already mentioned.

Figure 11 – Comparison of the evolution of the drag coefficient as a function of the angle of attack for the three wing and horizontal empennage combinations.

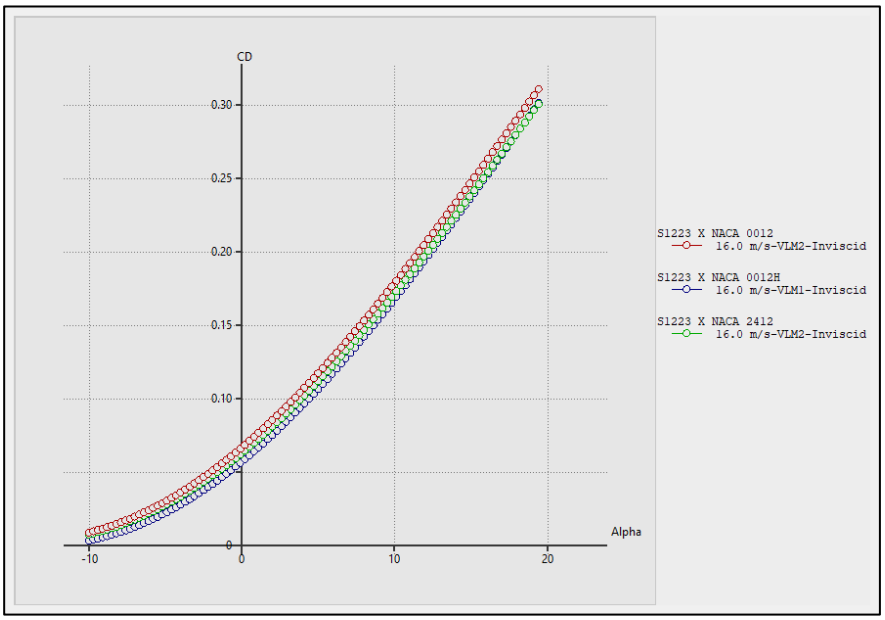

Source: Software XFLR5

By looking at the drag diagram, it can be seen that the three combinations present a linear variation of the drag coefficient with the angle of attack when α it is between approximately 5° and 20°. The *combination of S1223 RTL* and *NACA 0012H* is the one with the lowest drag coefficient values. The value of the maximum drag coefficient, *CDmax,* for each of the combinations is shown in Table 6.

Table 6 – Maximum drag coefficients for the three calculated configurations.

Configuration	**Maximum drag coefficient (*CDmax*)**
S1223 RTL e NACA 0012H	0.300
S1223 RTL e NACA 0012	0.310
S1223 RTL e NACA 2412	0.301

Source: The authors

Momentum Coefficients

Another important coefficient is the coefficient of momentum, which is responsible for the static stability of the aircraft, as mentioned above. Figure 12 shows the evolution of the moment coefficient *Cm*, with the angle of attack α, for the three configurations. In the three configurations, the pitch moment coefficient is negative, that is, in the direct direction, which demonstrates a static stability trend, generated by the pitch moment which, according to ANAC (ANACPÉDIA, 2024) is *the movement of an aircraft around the Y axis or the lateral axis* that opposes the rise movement of the aircraft's nose, when subjected to greater angles of attack. This moment, which causes a downward movement of the aircraft's nose, will help restore the aircraft to its original flight position in the event of a disturbance. On the other hand, the lower the moment coefficient value, the greater the static stability tendency of the aircraft.

Figure 12 – Comparison of the evolution of the moment coefficient as a function of the angle of attack for the three wing and horizontal empennage combinations.

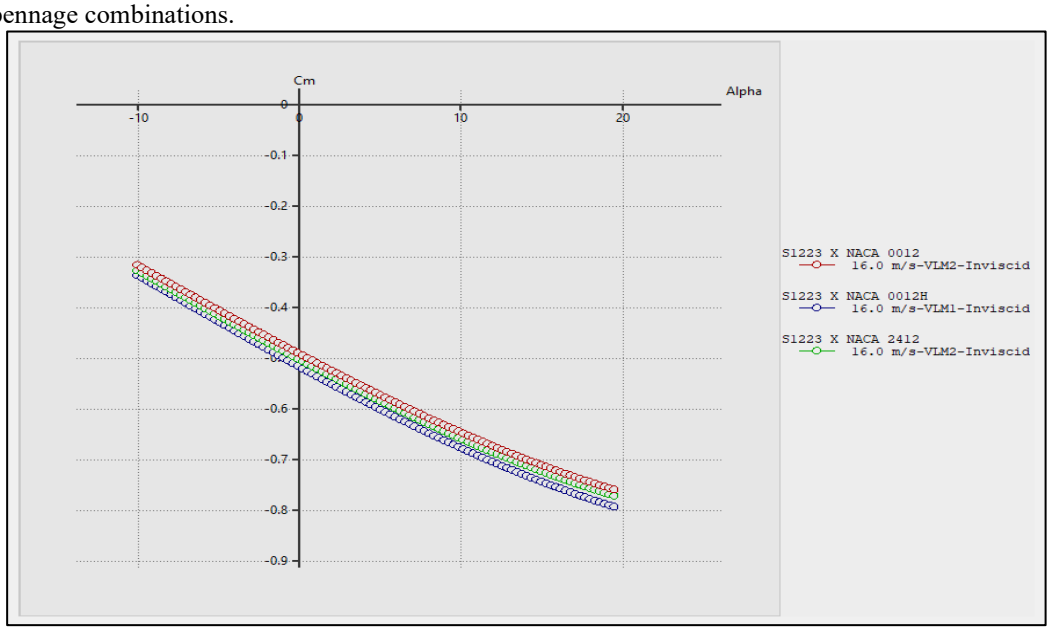

Source: Software XFLR5

Similarly, the lower the momentum coefficient, the greater the static stability tendency of the aircraft. The choice of the *S1223* and *NACA 0012H configuration,* which presents more efficient moment coefficients compared to the others, will be the right choice. Table 7 shows the maximum values of the moment coefficient for each configuration.

Table 7 – Maximum moment coefficients, in absolute value, for the three calculated configurations.

Configuration	**MAXIMUM DRAG COEFFICIENT (*cmmax*)**
S1223 RTL e NACA 0012H	-0.792
S1223 RTL e NACA 0012	-0.758
S1223 RTL e NACA 2412	-0.770

Source: The authors

Aerodynamic Efficiency

Aerodynamic efficiency εrelates the values of lift and drag coefficients, and is defined by the *CL*/*CD* ratio. Figure 13 shows the evolution of this coefficient ε with the angle of attack for the three configurations.

Figure 13 – Comparison of the evolution of aerodynamic efficiency, as a function of angle of attack, for the three wing and horizontal empennage combinations.

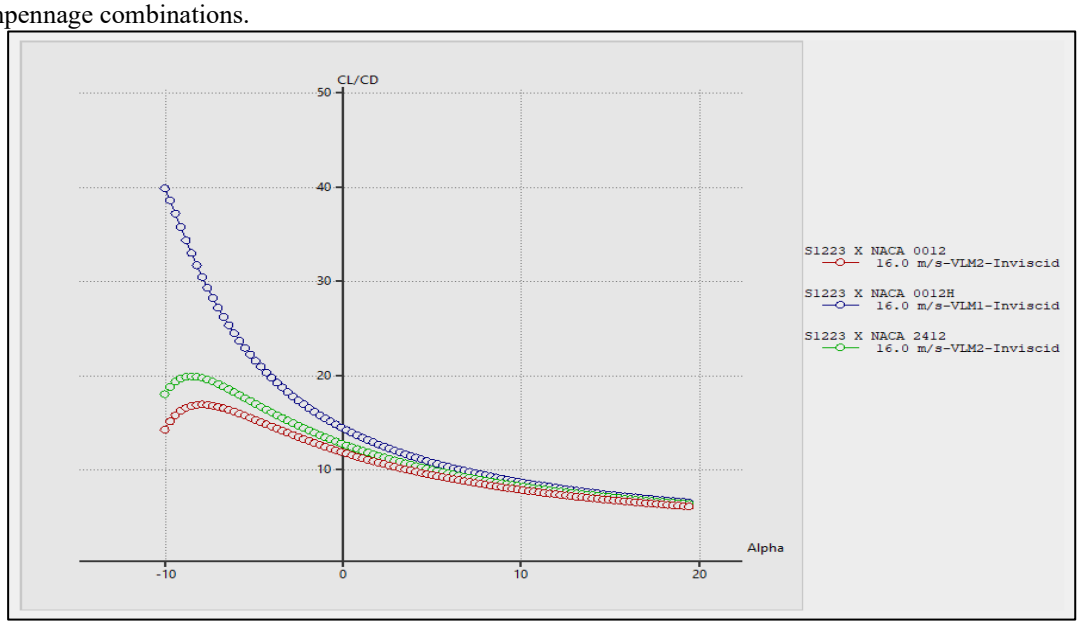

Source: Software XFLR5

For this analysis, it was observed among the curves of the three proposed models the curve that presents the highest values, that is, the angle of attack for which the lift is greater with less drag. In this way, it is possible to identify which configuration has the highest efficiency as a function of the angulation variation.

For positive angles of attack and greater than 5° degrees, the evolution of efficiency with the angle of attack is similar, being slightly better for the *NACA 0012H* profile. As the angle decreases and in particular for negative angles of attack, the difference increases, with the configuration with the NACA 0012H profile showing the highest values. Table 8 shows the maximum efficiency values for each configuration.

Table 8 – Maximum aerodynamic efficiency for the three calculated configurations.

Configuration	**Maximum aerodynamic efficiency (ε_{max})**
S1223 RTL e NACA 0012H	39.816
S1223 RTL e NACA 0012	16.848
S1223 RTL e NACA 2412	19.845

Source: The authors

CONCLUSION

The three-dimensional flow around the wing, the horizontal empennage and the wing-empennage joint configuration were calculated using the vortex mesh method, VLM, using the XFLR5 code. The wing is of the rectangular type, with a wingspan of 2.0 m and an aspect ratio of 4. The profile chosen for the wing was the SELIG 1223 RTL. The horizontal empennage is also of the rectangular type, it has a wingspan of 0.4 m and an aspect ratio of 2. For the empennage, three different profiles with a relative

thickness of 12% were considered: NACA 0012, NACA 0012H and NACA2412.

Results are presented regarding the evolution of lift coefficients *CL*, drag *CD*, *moment CM* and aerodynamic efficiency ε, as a function of angle of attack α, for the wing calculated separately, for the three horizontal empennage configurations and for the three combined wing and horizontal empennage configurations.

The three combinations of wing and empennage present good values regarding the evolution of lift, drag and moment coefficients. Regarding aerodynamic efficiency, the combination using the NACA 0012H profile shows better results, especially for negative angles of attack.

ACKNOWLEDGMENT

We would like to thank the Federal Rural University of the Semi-Arid Region for the financial support given for the development of the work presented in this article.

REFERENCES

AGÊNCIA NACIONAL DE AVIAÇÃO CIVIL ANAC. ANACPÉDIA, 2024. Disponível em: <https://www2.anac.gov.br/anacpedia/por-esp/tr3803.htm\>. Acesso em: 04 abr. 2024.

AIRFOIL TOOLS. Disponível em: <http://www.airfoiltools.com\>. Acesso em: 22 fev. 2024.

ANDERSON, John D. Fundamentals of Aerodynamics, 5. ed. McGraw-Hill, Nova York, 2010.

BREDERODE, Vasco. Aerodinâmica Incompressível. Fundamentos, 2. ed. Lisboa: Coleção Ensino da Ciência e da Tecnologia, 2018. 752 p.

DRELA, M.; YOUNG, H. XFOIL, 2001. Disponível em: <https://web.mit.edu/drela/Public/web/xfoil/xfoil_doc.txt\>. Acesso em: 08 mar. 2024.

DRELA, Mark. "An Analysis and Design System for Low Reynolds Number Airfoils." In: Low Reynolds Number Aerodynamics. Springer Berlin Heidelberg, 1989. p. 1-12.

HESS, J. L.; SMITH, A. M. O. "Calculation of potential flow about arbitrary bodies." Progress in Aerospace Sciences, v. 8, n. 1, 1966, p. 1-138.

HIRSH, C. Numerical Computation of Internal and External Flows. The Fundamentals of Computational Fluid Dynamics, 2ª Ed. Elsevier, EUA, 2007. 700 p.

RODRIGUES, Luís Eduardo Miranda José. Fundamentos da Engenharia Aeronáutica Aplicações ao Projeto SAE-AERODESIGN, 1. ed. São Paulo: Edição do Autor, 2011. 554 p.

SCORBILLI, R. Engenharia Aeronáutica. Porque o avião voa?, 2018. Disponível em: <https://engenhariaaeronautica.com.br/curiosidades-engenharia-aeronautica/por-que-o-aviao-voa/\>. Acesso em: 05 mar. 2022.

SHELDAHL, R. E. S.; KLIMAS, P. C. "Aerodynamic Characteristics of Seven Symmetrical Airfoil Sections Through 180-Degree Angle of Attack for Use in Aerodynamic Analysis of Vertical Axis Wind Turbines." Sandia National Laboratories, SANDS0-2114, 1981. 124 p.

THOMAS, James L. Vortex-lattice utilization. NASA SP-405, NASA-Langley, Washington, 1976. 423 p.

XFLR5. Versão 6.99. Disponível em: <http://www.xflr5.tech/xflr5.htm\>. Acesso em: 08 mar. 2024.